

(昭和 57 年 11 月 日本造船学会秋季講演会において講演)

Numerical Analysis of Free Surface Shock Waves around Bow by Modified MAC-Method

(Second Report)

by Akira Masuko*, *Member* Hideaki Miyata**, *Member*
Hisashi Kajitani**, *Member*

Summary

Computational schemes and numerical stability conditions of a modified version of Marker and Cell method are studied and a new computing program is developed using second-order upstream differencing representations of the momentum conservation equations and a SOR iterative method for solving a Poisson equation for the pressure, which is applicable to 3-D wave making problems of steadily advancing floating bodies in deep water. Computed results are given for nonlinear bow-waves of wedge models.

1. Introduction

Recently it is recognized that the wave making in the near-field of an advancing ship in deep water has nonlinear properties, which are analogous to those of waves that involve discontinuity. It is important to theoretically explain the nonlinear wave making, although familiar potential theories cannot be applied. For the nonlinear wave motion a numerical solution method is often very useful, and the MAC method is one of the most successful techniques for such problems. It is a technique for solving the time dependent Eulerian or Navier-Stokes equations of incompressible hydrodynamics and is suited for flows containing free surface. The method is based on finite difference representations of time dependent partial differential equations of momentum conservation.

In the previous paper¹⁾ the MAC method is employed for the present problem and it is modified and improved so as to cope with the problem of 3-D wave making around steadily advancing ship-bows in deep water. The modified version of the MAC method is called TUMMAC method.^{1),2)}

The TUMMAC method in the previous paper

is based on centered difference representation of the momentum equation and it necessitates artificial viscosity to stabilize the solution. Besides, the Poisson equation is solved by the Richardson's method with a relaxation factor less than unity. These give some difficulties in applications to various wave phenomena and result in slow convergence of the solution.

In this report, the MAC algorithm is briefly reviewed in Chapter 2. The centered and the second-order upstream difference representations for the momentum conservation equations are compared, and their numerical stability conditions are examined in Chapter 3. The Richardson's method and the SOR method for solving a Poisson equation for the pressure are examined in Chapter 4, and a new computing program is composed, which employs the second-order upstream differencing and the SOR method, in Chapter 5. Nonlinear wave formations around bows of wedge models, whose half-entrance angles are 20° and 45°, are computed by the new computer program at various advance speed in Chapter 6. The details of the experimental investigation into the characteristics of waves around bows of wedge models can be seen in Ref. 3).

The TUMMAC method for wedge models is called TUMMAC-I so that it is distinguished from the TUMMAC method for wall-sided ships of arbitrary waterlines, which is under development and is to be called TUMMAC-II.

The variables are as defined in Chapter 2 of

* Graduate School, Department of Naval Architecture, The University of Tokyo (present affiliation is Research Institute, IHI)

** Department of Naval Architecture, The University of Tokyo

the previous paper unless otherwise defined.

2. The MAC algorithm

The algorithm of the MAC method which is common to the TUMMAC method is briefly described for convenience.

The Navier-Stokes equations in conservative form are,

$$\left. \begin{aligned} \frac{\partial u}{\partial t} + \frac{\partial(u^2)}{\partial x} + \frac{\partial(uv)}{\partial y} + \frac{\partial(uw)}{\partial z} \\ = -\frac{\partial\psi}{\partial x} + \nu\left(\frac{\partial^2 u}{\partial x^2} + \frac{\partial^2 u}{\partial y^2} + \frac{\partial^2 u}{\partial z^2}\right) \\ \frac{\partial v}{\partial t} + \frac{\partial(uv)}{\partial x} + \frac{\partial(v^2)}{\partial y} + \frac{\partial(vw)}{\partial z} \\ = -\frac{\partial\psi}{\partial y} + \nu\left(\frac{\partial^2 v}{\partial x^2} + \frac{\partial^2 v}{\partial y^2} + \frac{\partial^2 v}{\partial z^2}\right) \\ \frac{\partial w}{\partial t} + \frac{\partial(uw)}{\partial x} + \frac{\partial(vw)}{\partial y} + \frac{\partial(w^2)}{\partial z} \\ = -\frac{\partial\psi}{\partial z} + \nu\left(\frac{\partial^2 w}{\partial x^2} + \frac{\partial^2 w}{\partial y^2} + \frac{\partial^2 w}{\partial z^2}\right) + g \end{aligned} \right\} (1)$$

By forward differencing in time and centered differencing in space, Eqs. (1) become,

$$\left. \begin{aligned} \frac{u_{i+(1/2)jk}^{n+1} - u_{i+(1/2)jk}^n}{DT} \\ = -UC_{i+(1/2)jk} - \frac{\psi_{i+1jk} - \psi_{ijk}}{DX} \\ + \nu \left[\frac{u_{i+(3/2)jk} + u_{i-(1/2)jk} - 2u_{i+(1/2)jk}}{DX^2} \right. \\ + \frac{u_{i+(1/2)j+1k} + u_{i+(1/2)j-1k} - 2u_{i+(1/2)jk}}{DY^2} \\ \left. + \frac{u_{i+(1/2)jk+1} + u_{i+(1/2)jk-1} - 2u_{i+(1/2)jk}}{DZ^2} \right] \\ \frac{v_{ij+(1/2)k}^{n+1} - v_{ij+(1/2)k}^n}{DT} \\ = -VC_{ij+(1/2)k} - \frac{\psi_{ij+1k} - \psi_{ijk}}{DY} + \dots \\ \frac{w_{ijk+1/2}^{n+1} - w_{ijk+1/2}^n}{DT} \\ = -WC_{ijk+1/2} - \frac{\psi_{ijk+1} - \psi_{ijk}}{DZ} + g + \dots \end{aligned} \right\} (2)$$

In the above equations subscripts are used for the cell location and superscripts for the time level. Variables with superscript $(n+1)$ are related to the $(n+1)$ -th time step and variables lacking a superscript are evaluated at the n -th step. The convection terms are denoted UC , VC and WC whose expression is described in the following chapter.

The expression for the velocity components at the $(n+1)$ -th time step is derived by combining the terms except the pressure gradient term and denoting them ξ , η and ζ .

$$\left. \begin{aligned} u_{i+(1/2)jk}^{n+1} &= \xi_{i+(1/2)jk} - \frac{\psi_{i+1jk} - \psi_{ijk}}{DX} DT \\ v_{ij+(1/2)k}^{n+1} &= \eta_{ij+(1/2)k} - \frac{\psi_{ij+1k} - \psi_{ijk}}{DY} DT \\ w_{ijk+1/2}^{n+1} &= \zeta_{ijk+1/2} - \frac{\psi_{ijk+1} - \psi_{ijk}}{DZ} DT \end{aligned} \right\} (3)$$

The divergence at the $(n+1)$ -th time step is obtained from Eqs. (3) as,

$$\begin{aligned} D_{ijk}^{n+1} &= \frac{u_{i+(1/2)jk}^{n+1} - u_{i-(1/2)jk}^{n+1}}{DX} + \frac{v_{ij+(1/2)k}^{n+1} - v_{ij-(1/2)k}^{n+1}}{DY} \\ &\quad + \frac{w_{ijk+1/2}^{n+1} - w_{ijk-1/2}^{n+1}}{DZ} \\ &= \frac{\xi_{i+(1/2)jk} - \xi_{i-(1/2)jk}}{DX} + \frac{\eta_{ij+(1/2)k} - \eta_{ij-(1/2)k}}{DY} \\ &\quad + \frac{\zeta_{ijk+1/2} - \zeta_{ijk-1/2}}{DZ} \\ &\quad + \frac{DT}{DX^2} [2\psi_{ijk} - \psi_{i+1jk} - \psi_{i-1jk}] \\ &\quad + \frac{DT}{DY^2} [2\psi_{ijk} - \psi_{ij+1k} - \psi_{ij-1k}] \\ &\quad + \frac{DT}{DZ^2} [2\psi_{ijk} - \psi_{ijk+1} - \psi_{ijk-1}] \end{aligned} \quad (4)$$

$D=0$ is required to rigorously conserve mass and it is aimed at at the $(n+1)$ -th time step, i.e., D_{ijk}^{n+1} in Eq. (4) is set zero. Then, the equation for the pressure is derived as,

$$\left. \begin{aligned} \psi_{ijk} &= \frac{1}{2\left(\frac{1}{DX^2} + \frac{1}{DY^2} + \frac{1}{DZ^2}\right)} \\ &\quad \cdot \left[\frac{\psi_{i+1jk} + \psi_{i-1jk}}{DX^2} + \frac{\psi_{ij+1k} + \psi_{ij-1k}}{DY^2} \right. \\ &\quad \left. + \frac{\psi_{ijk+1} + \psi_{ijk-1}}{DZ^2} - R_{ijk} \right] \end{aligned} \right\} (5)$$

where

$$\begin{aligned} R_{ijk} &= \frac{\xi_{i+(1/2)jk} - \xi_{i-(1/2)jk}}{DT \cdot DX} + \frac{\eta_{ij+(1/2)k} - \eta_{ij-(1/2)k}}{DT \cdot DY} \\ &\quad + \frac{\zeta_{ijk+1/2} - \zeta_{ijk-1/2}}{DT \cdot DZ} \end{aligned}$$

Since R_{ijk} is determined when u , v and w are given, Eq. (5) is a Poisson equation for the pressure.

The momentum equations (3) and the Poisson equation (5) are the principal equations to be solved. Eqs. (3) are hyperbolic equations which are solved as an initial value problem and Eq. (5) is an elliptic equation which is solved as a boundary value problem.

The solution is advanced in time by a series of repeated steps. First the Poisson equation (5) is iteratively solved under given initial boundary conditions and then new velocity components

are derived from the momentum equations (3). A new source term R_{ijk} for the Poisson equation is calculated by the new velocity fields and the cycle is repeated. Marker particles are used to tell the new location of free surface. This solution algorithm is suitable to unsteady problems, although it is applied to a steady wave making problem in this paper by letting an unsteady solution approach to a steady state.

3. FTCS and donor-cell methods

In the previous paper the FTCS (forward-time, centered-space differencing) method was applied and it necessitated the introduction of artificial viscosity.

There are some alternatives for the finite-difference representation of the convection terms, and the donor-cell (second-order upstream differencing) method is chosen for the improved TUMMAC-I method in this report. The properties of solutions remarkably depend on the differencing scheme, as finite-difference representations are approximations to the original differential equations.

In this chapter numerical stability, degree of accuracy and transporative property are examined for the centered differencing applied in the previous paper and the donor-cell method applied to the improved TUMMAC-I. For simplicity the property of the upstream differencing scheme is studied with the first-order representation instead of the second-order one, i.e., donor-cell method.

3.1 Finite-difference representation of convective terms

Let us compare finite difference representations of the convective terms of the Navier-Stokes equations (UC , VC and WC in Eq. (2)). UC is chosen as a typical example and the descriptions of VC and WC are abbreviated here.

By centered differencing,

$$UC_{i+(1/2)jk} = \frac{1}{DX} [(u^2)_{i+1jk} - (u^2)_{ijk}] + \frac{1}{DY} [(uv)_{i+(1/2)j+(1/2)k} - (uv)_{i+(1/2)j-(1/2)k}] + \frac{1}{DZ} [(uw)_{i+(1/2)jk+1/2} - (uw)_{i+(1/2)jk-1/2}]$$

where

$$(u^2)_{ijk} = \frac{1}{4} (u_{i+(1/2)jk} + u_{i-(1/2)jk})^2$$

$$(uv)_{i+(1/2)j+(1/2)k} = \frac{1}{4} (u_{i+(1/2)jk} + u_{i+(1/2)j+1k}) \cdot (v_{i+j+(1/2)k} + v_{i+j+(1/2)k})$$

$$(uw)_{i+(1/2)jk+1/2} = \frac{1}{4} (u_{i+(1/2)jk} + u_{i+(1/2)jk+1}) \cdot (w_{ijk+1/2} + w_{i+(1/2)jk+1/2})$$

(6)

The upstream differencing depends on the flow direction and by the first-order upstream differencing UC becomes,

$$UC_{i+(1/2)jk} = \frac{1}{DX} \left[(u^2)_{i+(1/2)jk} - \begin{cases} (u^2)_{i-(1/2)jk} & \text{if } u_{i+(1/2)jk} > 0 \\ (u^2)_{i+(3/2)jk} & \text{if } u_{i+(1/2)jk} < 0 \end{cases} \right] + \frac{1}{DY} \left[(uv)_{i+(1/2)jk} - \begin{cases} (uv)_{i+(1/2)j-1k} & \text{if } v_{i+(1/2)jk} > 0 \\ (uv)_{i+(1/2)j+1k} & \text{if } v_{i+(1/2)jk} < 0 \end{cases} \right] + \frac{1}{DZ} \left[(uw)_{i+(1/2)jk} - \begin{cases} (uw)_{i+(1/2)jk-1} & \text{if } w_{i+(1/2)jk} > 0 \\ (uw)_{i+(1/2)jk+1} & \text{if } w_{i+(1/2)jk} < 0 \end{cases} \right]$$

where

$$u_{i+j+(1/2)k} = \frac{1}{4} (u_{i+(1/2)jk} + u_{i-(1/2)jk} + u_{i+(1/2)j+1k} + u_{i-(1/2)j+1k})$$

(7)

The first-order upstream differencing scheme violates the conservative property in the region where reverse flow exists and this shortcoming can be resolved by the second-order upstream differencing in which, for example, velocity component u for the x -directional gradient is estimated at the mid-point of the velocity points.⁴⁾ (see Fig. 1) This differencing method is called donor-cell method and written as,

$$UC_{i+(1/2)jk} = \frac{1}{DX} [u_{i+1jk} u_{XR} - u_{ijk} u_{XL}] + \frac{1}{DY} [v_{i+(1/2)j+(1/2)k} u_{YR} - v_{i+(1/2)j-(1/2)k} u_{YL}] + \frac{1}{DZ} [w_{i+(1/2)jk+1/2} u_{ZR} - w_{i+(1/2)jk-1/2} u_{ZL}]$$

where

$$u_{XR} = \begin{cases} u_{i+(1/2)jk} & \text{if } u_{i+1jk} > 0 \\ u_{i+(3/2)jk} & \text{if } u_{i+1jk} < 0 \end{cases}$$

$$u_{XL} = \begin{cases} u_{i-(1/2)jk} & \text{if } u_{ijk} > 0 \\ u_{i+(1/2)jk} & \text{if } u_{ijk} < 0 \end{cases}$$

$$u_{YR} = \begin{cases} u_{i+(1/2)jk} & \text{if } v_{i+(1/2)j+(1/2)k} > 0 \\ u_{i+(1/2)j+1k} & \text{if } v_{i+(1/2)j+(1/2)k} < 0 \end{cases}$$

$$u_{YL} = \begin{cases} u_{i+(1/2)j-1k} & \text{if } v_{i+(1/2)j-(1/2)k} > 0 \\ u_{i+(1/2)jk} & \text{if } v_{i+(1/2)j-(1/2)k} < 0 \end{cases}$$

$$u_{ZR} = \begin{cases} u_{i+(1/2)jk} & \text{if } w_{i+(1/2)jk+1/2} > 0 \\ u_{i+(1/2)jk+1} & \text{if } w_{i+(1/2)jk+1/2} < 0 \end{cases}$$

$$u_{ZL} = \begin{cases} u_{i-(1/2)jk-1} & \text{if } w_{i+(1/2)jk-1/2} > 0 \\ u_{i+(1/2)jk} & \text{if } w_{i+(1/2)jk-1/2} < 0 \end{cases}$$

(8)

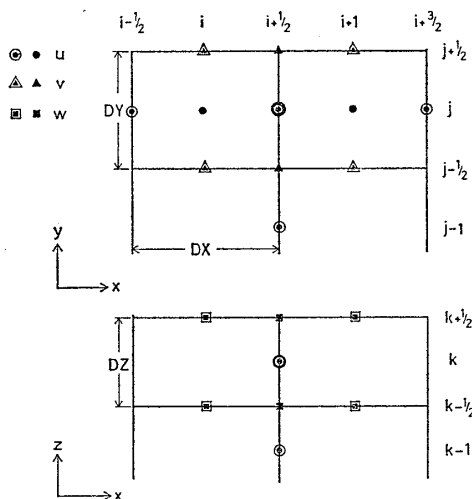


Fig. 1 Velocity points for the second-order upstream differencing (*u*-component)

3.2 Numerical stability analysis

Conditions required in order to obtain stabilized solutions are examined. The Nuemann's method of stability analysis^{4),5)} is applied. This method is valid for linear equations, and therefore, the finite-difference equations are linearized by assumptions. And besides, a pressure gradient term and a gravitational term are ignored. Thus, this analysis gives only approximate conditions.

The convective terms of Eq. (2) are expressed by centered differencing and the pressure gradient and gravitational terms are neglected, and then, the model equation for the centered differencing scheme becomes,

$$\begin{aligned}
 q_{lmn}^{n+1} = & q_{lmn} + \frac{DT}{DX} [(uq)_{l-(1/2)mn} - (uq)_{l+(1/2)mn}] \\
 & + \frac{DT}{DY} [(vq)_{lm-(1/2)n} - (vq)_{lm+(1/2)n}] \\
 & + \frac{DT}{DZ} [(wq)_{lmn-1/2} - (wq)_{lmn+1/2}] \\
 & + \nu DT \left[\frac{q_{l+1mn} + q_{l-1mn} - 2q_{lmn}}{DX^2} \right. \\
 & + \frac{q_{lm+1n} + q_{lm-1n} - 2q_{lmn}}{DY^2} \\
 & \left. + \frac{q_{lmn+1} + q_{lmn-1} - 2q_{lmn}}{DZ^2} \right]
 \end{aligned}$$

where

$$\begin{aligned}
 l = i + 1/2 \quad m = j \quad n = k & \quad \text{if } q = u \\
 l = i \quad m = j + 1/2 \quad n = k & \quad q = v \\
 l = i \quad m = j \quad n = k + 1/2 & \quad q = w \\
 u_{ijk} = \frac{1}{2} (u_{i-(1/2)jk} + u_{i+(1/2)jk}), \text{ etc.}
 \end{aligned}$$

(9)

Note that *n* is as defined above unless it is used

as a superscript denoting time step in this section. The right-hand-side terms are evaluated at the *n*-th time step. Eq. (9) is linearized by substituting *u_{lmn}*, *v_{lmn}* and *w_{lmn}* for *u*, *v* and *w*, respectively, and assuming them constants. Then Eq. (9) becomes,

$$\begin{aligned}
 q_{lmn}^{n+1} = & q_{lmn} + \frac{c_x}{2} (q_{l-1mn} - q_{l+1mn}) \\
 & + \frac{c_y}{2} (q_{lm-1n} - q_{lm+1n}) + \frac{c_z}{2} (q_{lmn-1} - q_{lmn+1}) \\
 & + d_x (q_{l+1mn} + q_{l-1mn} - 2q_{lmn}) \\
 & + d_y (q_{lm+1n} + q_{lm-1n} - 2q_{lmn}) \\
 & + d_z (q_{lmn+1} + q_{lmn-1} - 2q_{lmn})
 \end{aligned} \tag{10}$$

in which *c_x*, *c_y* and *c_z* are Courant numbers and *d_x*, *d_y* and *d_z* are diffusion numbers in three directions defined as,

$$\left. \begin{aligned}
 c_x = \frac{DT u_{lmn}}{DX}, \quad c_y = \frac{DT v_{lmn}}{DY} \\
 c_z = \frac{DT w_{lmn}}{DZ}, \quad d_x = \frac{DT \nu}{DX^2} \\
 d_y = \frac{DT \nu}{DY^2}, \quad d_z = \frac{DT \nu}{DZ^2}
 \end{aligned} \right\} \tag{11}$$

Assume that the solution is expressed by a Fourier series whose component is,

$$\begin{aligned}
 q_{lmn} = & V e^{I(k_x l DX + k_y m DY + k_z n DZ)} \\
 = & V e^{I(l\theta_x + m\theta_y + n\theta_z)}
 \end{aligned} \tag{12}$$

in which *I* is the imaginary unit and *k_x*, *k_y*, *k_z* and *θ_x*, *θ_y*, *θ_z* are wave numbers and phase angles. By substituting Eq. (12) into Eq. (10),

$$\begin{aligned}
 V^{n+1} = & V^n + V^n \left(c_x \frac{e^{-I\theta_x} - e^{I\theta_x}}{2} \right. \\
 & + c_y \frac{e^{-I\theta_y} - e^{I\theta_y}}{2} + c_z \frac{e^{-I\theta_z} - e^{I\theta_z}}{2} \\
 & + V^n [d_x (e^{I\theta_x} + e^{-I\theta_x} - 2) \\
 & + d_y (e^{I\theta_y} + e^{-I\theta_y} - 2) \\
 & \left. + d_z (e^{I\theta_z} + e^{-I\theta_z} - 2) \right]
 \end{aligned} \tag{13}$$

Eq. (13) is rewritten as,

$$\begin{aligned}
 V^{n+1} = & G V^n \\
 G = & 1 + 2 [d_x (\cos \theta_x - 1) + d_y (\cos \theta_y - 1) \\
 & + d_z (\cos \theta_z - 1)] \\
 & - I (c_x \sin \theta_x + c_y \sin \theta_y + c_z \sin \theta_z)
 \end{aligned} \tag{14}$$

|*G*| ≤ 1 is required for any value of *θ_x*, *θ_y* and *θ_z* to assure stability of solutions. This leads to the following stability condition.

$$(c_x + c_y + c_z)^2 \leq 2(d_x + d_y + d_z) \leq 1$$

that is,

$$\left. \begin{aligned}
 \left(\frac{DT u_{lmn}}{DX} + \frac{DT v_{lmn}}{DY} + \frac{DT w_{lmn}}{DZ} \right)^2 \\
 \leq 2 \left(\frac{\nu DT}{DX^2} + \frac{\nu DT}{DY^2} + \frac{\nu DT}{DZ^2} \right) \leq 1
 \end{aligned} \right\} \tag{15}$$

Stabilized solutions cannot be derived by the centered differencing method unless artificial viscosity is introduced. In other words, Eulerian equations cannot be solved by this method. The required value of kinematic viscosity ν is bounded by upper and lower limits.

Assume that u_{lmn} , v_{lmn} and w_{lmn} are all half of the uniform stream velocity U , and then, Eq. (15) becomes,

$$\frac{DT^2 U^2}{4} \left(\frac{1}{DX} + \frac{1}{DY} + \frac{1}{DZ} \right)^2 \leq 2\nu DT \left(\frac{1}{DX^2} + \frac{1}{DY^2} + \frac{1}{DZ^2} \right) \leq 1 \quad (16)$$

By introducing nondimensional time increment and Reynolds number,

$$\left. \begin{aligned} & \frac{8 \left(\frac{1}{DX^2} + \frac{1}{DY^2} + \frac{1}{DZ^2} \right)}{DTND \left(\frac{1}{DX} + \frac{1}{DY} + \frac{1}{DZ} \right)^2} \geq R_n \\ & \geq 2DTND \cdot d^2 \left(\frac{1}{DX^2} + \frac{1}{DY^2} + \frac{1}{DZ^2} \right) \end{aligned} \right\} \quad (17)$$

where
 $DTND = DT \cdot U/d$, $R_n = Ud/\nu$

The Courant condition, which implies that the fluid is not permitted to cross more than one cell in one time step, requires simultaneously the following upper limit of $DTND$.

$$DTND \leq \frac{2}{\left(\frac{1}{DX} + \frac{1}{DY} + \frac{1}{DZ} \right) d} \quad (18)$$

When cell dimensions are $DX=0.05$ m, $DY=0.018$ m and $DZ=0.025$ m, and U and d are 1.0 m/s and 0.1 m, respectively, as in the previous paper for a wedge model of $\alpha=20^\circ$, the required upper limit of $DTND$ is 0.17, and the required ranges of R_n are,

$$\left. \begin{aligned} 10 < R_n < 31 & \quad \text{when } DTND=0.10 \\ 1 < R_n < 305 & \quad \text{when } DTND=0.01 \end{aligned} \right\} \quad (19)$$

Thus, the centered differencing method necessitates the introduction of artificial viscosity.

The model equation for the first-order upstream differencing scheme is,

$$\begin{aligned} q_{lmn}^{n+1} = & q_{lmn} + \frac{DT}{DX} [(uq)_{l-1mn} - (uq)_{lmn}] \\ & + \frac{DT}{DY} [(vq)_{lm-1n} - (vq)_{lmn}] \\ & + \frac{DT}{DZ} [(wq)_{lmn-1} - (wq)_{lmn}] \\ & + \nu DT \left[\frac{q_{l+1mn} + q_{l-1mn} - 2q_{lmn}}{DX^2} \right. \end{aligned}$$

$$\left. + \frac{q_{lm+1n} + q_{lm-1n} - 2q_{lmn}}{DY^2} + \frac{q_{lmn+1} + q_{lmn-1} - 2q_{lmn}}{DZ^2} \right] \quad (20)$$

Eq. (20) is linearized by substituting $u_{l-(1/2)mn}$, $v_{lm-(1/2)n}$ and $w_{lmn-1/2}$ for u , v and w , respectively, and assuming them constants.

$$\begin{aligned} q_{lmn}^{n+1} = & q_{lmn} + c_x (q_{l-1mn} - q_{lmn}) \\ & + c_y (q_{lm-1n} - q_{lmn}) \\ & + c_z (q_{lmn-1} - q_{lmn}) \\ & + d_x (q_{l+1mn} + q_{l-1mn} - 2q_{lmn}) \\ & + d_y (q_{lm+1n} + q_{lm-1n} - 2q_{lmn}) \\ & + d_z (q_{lmn+1} + q_{lmn-1} - 2q_{lmn}) \end{aligned} \quad (21)$$

where

$$\left. \begin{aligned} c_x = \frac{DT u_{l-(1/2)mn}}{DX}, \quad c_y = \frac{DT v_{lm-(1/2)n}}{DY} \\ c_z = \frac{DT w_{lmn-1/2}}{DZ} \end{aligned} \right\} \quad (22)$$

Through the same procedure as the case of centered differencing above-described, the amplification factor is derived as,

$$\begin{aligned} G = & 1 + [(c_x + 2d_x)(\cos \theta_x - 1) \\ & + (c_y + 2d_y)(\cos \theta_y - 1) \\ & + (c_z + 2d_z)(\cos \theta_z - 1)] \\ & - I(c_x \sin \theta_x + c_y \sin \theta_y + c_z \sin \theta_z) \end{aligned} \quad (23)$$

Stability condition becomes,

$$(c_x + c_y + c_z)^2 \leq (c_x + c_y + c_z) + 2(d_x + d_y + d_z) \leq 1 \quad (24)$$

Eq. (24) is decomposed into the following two conditions.

$$c_x + c_y + c_z \leq 1 \quad (25)$$

$$\begin{aligned} 2\nu DT \left(\frac{1}{DX^2} + \frac{1}{DY^2} + \frac{1}{DZ^2} \right) \\ \leq 1 - (c_x + c_y + c_z) \end{aligned} \quad (26)$$

The former is the Courant condition and the latter imposes an upper limit of kinematic viscosity.

The lower limit of Reynolds number is estimated by the values used to obtain Eq. (19) as follows.

$$\left. \begin{aligned} R_n > 27 & \quad \text{when } DTND=0.10 \\ R_n > 1.1 & \quad \text{when } DTND=0.01 \end{aligned} \right\} \quad (27)$$

The linearized model equation for the donor-cell method is,

$$\begin{aligned} q_{lmn}^{n+1} = & q_{lmn} + c_x (q_{l-1mn} - q_{lmn}) \\ & + c_y (q_{lm-1n} - q_{lmn}) \\ & + c_z (q_{lmn-1} - q_{lmn}) \end{aligned}$$

$$\begin{aligned}
& +d_x(q_{l+1mn}+q_{l-1mn}-2q_{lmn}) \\
& +d_y(q_{lm+1n}+q_{lm-1n}-2q_{lmn}) \\
& +d_z(q_{lmn+1}+q_{lmn-1}-2q_{lmn}) \quad (28)
\end{aligned}$$

in which Courant numbers and diffusion numbers are defined in the same manner with the centered differencing scheme.

Eq. (28) is quite the same with Eq. (21), and therefore, the stability conditions for the donor-cell method is supposed to be nearly equivalent to those of the first-order upstream differencing method. The upstream differencing does not necessitate artificial viscosity.

It must be noted that the present analysis of numerical stability gives only approximate conditions, because it is based on the simplification of the equations. The computation of waves around a wedge model of $\alpha=20^\circ$ by FTCS method gives stable results when $R_n=50$ and $DTND=0.01$, while it gives unstable ones when $R_n=200$ and $DTND=0.01^2$. Both values of R_n are within the stable range of Eq. (19).

3.3 Degree of accuracy and transporative property

Finite-difference representations of the momentum equations are approximations to the differential equation, and the degree of accuracy depends on the way of finite-differencing. The accuracy analysis⁴⁾ shows that the centered differencing of the convective terms possesses second-order accuracy, i.e., the error due to the approximation is the order of cell length squared and that the first-order upstream differencing possesses only first-order accuracy. The degree of accuracy of the donor-cell method is supposed to be in between.

It is also shown that the FTCS scheme implicitly includes negative diffusion terms which make solutions unstable and that the donor-cell scheme, on the contrary, implicitly includes positive diffusion terms which make the solution stable and simultaneously cause numerical dissipation.⁴⁾ Thus the donor-cell method gives smoothed solutions whose degree of accuracy is not greater than the centered differencing method, although it gives stable solution with less effort without artificial viscosity. The wave height computed by the donor-cell method is supposed to be lower than that in the previous paper computed by the centered differencing method.

When an influence of disturbance is conveyed only along the flow direction by the convection of a difference equation, this equation is said to have transporative property. It is desired for a differencing scheme of convection terms to possess transporative property. The centered differencing does not possess this property while the upstream differencing does,⁴⁾ and therefore,

the latter differencing, including the donor-cell method, is desirable in this respect.

4. Poisson equation for the pressure

4.1 Richardson's and Liebmann's methods

The Poisson equation (5) is iteratively solved by the following equation.

$$\psi_{ijk}^{m+1} = \psi_{ijk}^m + \omega(\psi_{ijk}^{m+1\text{cal}} - \psi_{ijk}^m) \quad (29)$$

ψ_{cal} is the value calculated by Eq. (5). The superscripts m and $(m+1)$ denote iteration number and ω is a relaxation factor. The iteration is continued until the difference of pressure between the $(m+1)$ -th and m -th steps converges within an allowable error.

The Richardson's method which was used in the previous paper is described as,

$$\begin{aligned}
\psi_{ijk}^{m+1} = & \frac{1}{2\left(\frac{1}{DX^2} + \frac{1}{DY^2} + \frac{1}{DZ^2}\right)} \\
& \cdot \left[\frac{\psi_{i+1jk}^m + \psi_{i-1jk}^m}{DX^2} + \frac{\psi_{ij+1k}^m + \psi_{ij-1k}^m}{DY^2} \right. \\
& \left. + \frac{\psi_{ijk+1}^m + \psi_{ijk-1}^m}{DZ^2} - R_{ijk} \right] \quad (30)
\end{aligned}$$

All the pressures on the right-hand-side are evaluated at the previous m -th step.

The Liebmann's method uses the new pressures successively obtained at the $(m+1)$ -th step as seen in Fig. 2 and writes,

$$\begin{aligned}
\psi_{ijk}^{m+1} = & \frac{1}{2\left(\frac{1}{DX^2} + \frac{1}{DY^2} + \frac{1}{DZ^2}\right)} \\
& \cdot \left[\frac{\psi_{i+1jk}^m + \psi_{i-1jk}^{m+1}}{DX^2} + \frac{\psi_{ij+1k}^m + \psi_{ij-1k}^{m+1}}{DY^2} \right. \\
& \left. + \frac{\psi_{ijk+1}^m + \psi_{ijk-1}^{m+1}}{DZ^2} - R_{ijk} \right] \quad (31)
\end{aligned}$$

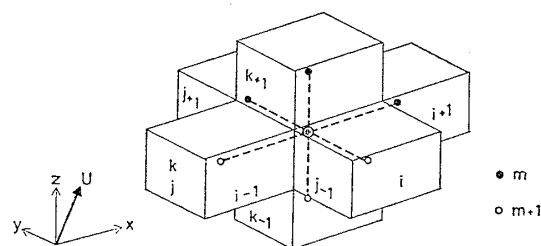


Fig. 2 Pressure points for SOR method

4.2 Numerical stability analysis

Numerical stability of the Richardson's method is examined by substituting Eq. (30) into Eq. (29).

$$\psi_{ijk}^{m+1} = (1-\omega)\psi_{ijk}^m + \frac{\omega}{2\left(\frac{1}{DX^2} + \frac{1}{DY^2} + \frac{1}{DZ^2}\right)}$$

$$\cdot \left[\frac{\psi_{i+1jk}^m + \psi_{i-1jk}^m}{DX^2} + \frac{\psi_{ij+1k}^m + \psi_{ij-1k}^m}{DY^2} + \frac{\psi_{ijk+1}^m + \psi_{ijk-1}^m}{DZ^2} - R_{ijk} \right] \quad (32)$$

The Neumann's analysis of numerical stability applied in Chaptre 3 is again applied to Eq. (32) and consequently the amplification function is derived as,

$$G = 1 - \omega(1 - \cos \theta) \quad (33)$$

Then, the stability condition requires the following range of the relaxation factor. Under-relaxation is required for the Richardson's method.

$$0 \leq \omega \leq 1 \quad (34)$$

For the case of the Liebmann's method, the relaxation equation and the amplification function are, respectively,

$$\begin{aligned} \psi_{ijk}^{m+1} = & (1 - \omega)\psi_{ijk}^m + \frac{\omega}{2 \left(\frac{1}{DX^2} + \frac{1}{DY^2} + \frac{1}{DZ^2} \right)} \\ & \cdot \left[\frac{\psi_{i+1jk}^m + \psi_{i-1jk}^{m+1}}{DX^2} + \frac{\psi_{ij+1k}^m + \psi_{ij-1k}^{m+1}}{DY^2} \right. \\ & \left. + \frac{\psi_{ijk+1}^m + \psi_{ijk-1}^{m+1}}{DZ^2} - R_{ijk} \right] \quad (35) \end{aligned}$$

$$G = \frac{1 - \omega + \frac{\omega e^{I\theta}}{2}}{1 - \frac{\omega e^{-I\theta}}{2}} \quad (36)$$

To secure stability the following range of the relaxation factor is required.

$$0 \leq \omega < 2 \quad (37)$$

One can obtain stabilized solution by over-relaxation when the Liebmann's method is used. The Liebmann's method which uses a relaxation factor greater than unity is called successive over-relaxation (SOR) method. Faster convergence of the SOR method can save computation time.

In the calculations in the previous paper the Richardson's method with $\omega = 0.3$ is employed and in the following chapters the SOR method with $\omega = 1.5$.

5. Improved TUMMAC-I computational program

The TUMMAC computational program for water flows around wedge models (TUMMAC-I) is improved so that stable state can be attained more easily with shorter computational time. The donor-cell method is applied to the difference representation of the convective terms and the SOR method to the solution of the Poisson equation for the pressure.

The computational procedure, the boundary

conditions, the initial conditions and the treatment of the marker particles of the improved version of TUMMAC-I are almost the same with the original in the previous paper. However, the description in that paper is too brief, and therefore some explanations are added below.

The initial state of computation is at rest and the inflow velocity is gradually accelerated until the assumed speed of advance of floating bodies is reached at about 100-th time step. To impulsively start the bodies does not give favorable rapid convergence.

The kinematic free surface condition is satisfied by the movement of marker particles and the dynamic free surface condition is satisfied by letting $P = P_0 = 0$ at the exact location of the free surface. The expression of the pressure near the free surface for 3-D case is given by 3-D "irregular stars" as,

$$\begin{aligned} P_{ijk} = & \frac{\eta_1 \eta_2 \eta_3 \eta_4 \eta_5 \eta_6}{\eta_1 \eta_2 \eta_3 \eta_4 + \eta_3 \eta_4 \eta_5 \eta_6 + \eta_1 \eta_2 \eta_5 \eta_6} \\ & \cdot \left[\frac{\eta_2 P_1 + \eta_1 P_2}{\eta_1 \eta_2 (\eta_1 + \eta_2)} + \frac{\eta_4 P_3 + \eta_3 P_4}{\eta_3 \eta_4 (\eta_3 + \eta_4)} \right. \\ & \left. + \frac{\eta_6 P_5 + \eta_5 P_6}{\eta_5 \eta_6 (\eta_5 + \eta_6)} - \frac{1}{2} \rho R \right] \quad (38) \end{aligned}$$

In this equation P on the right-hand-side is set zero for the cells on the free surface (see Fig. 1 (c) of the previous paper). The viscous effect on the free surface condition is not taken into account.

The velocity gradient along the local streamline is set zero at the outflow boundaries to prevent wave reflection. The computed flow field is connected to the previously calculated double model flow at a deep horizontal plane. The body boundary condition is a free-slip condition as described in the previous paper.

6. Computed waves around wedge models

The improved version of TUMMAC-I was applied to the calculation of waves generated by steadily advancing floating wedge models in deep water. The details of the characteristics of these waves are experimentally studied in Ref. 3).

6.1 Computational conditions

Two wedge models whose half-entrance angle (α) is 20° and 45° are chosen for the computation.

The length and depth of the wedge model of $\alpha = 20^\circ$ are 720 mm and 100 mm, respectively, and cell dimensions (DX, DY, DZ) are (36, 13, 25 mm). The number of cell is $32 \times 40 \times 12$. These values of the wedge model of $\alpha = 45^\circ$ are 400 mm and 100 mm, (DX, DY, DZ) = (25, 25, 25 mm) and $37 \times 27 \times 14$.

Waves are computed at three Froude numbers based on draft (F_d) for each model. The parameters used for the computations are listed in Table 1.

Table 1 Conditions of computations

	F_d	U (m/s)	DT (sec)	$DTND$	ν	ω
$\alpha = 20^\circ$	0.8	0.792	0.00631	0.05	0	1.5
	1.1	1.089	0.00459			
	1.4	1.386	0.00361			
$\alpha = 45^\circ$	0.6	0.594	0.00421	0.025	0	1.5
	0.8	0.792	0.00631	0.95		
	1.0	0.990	0.00505			

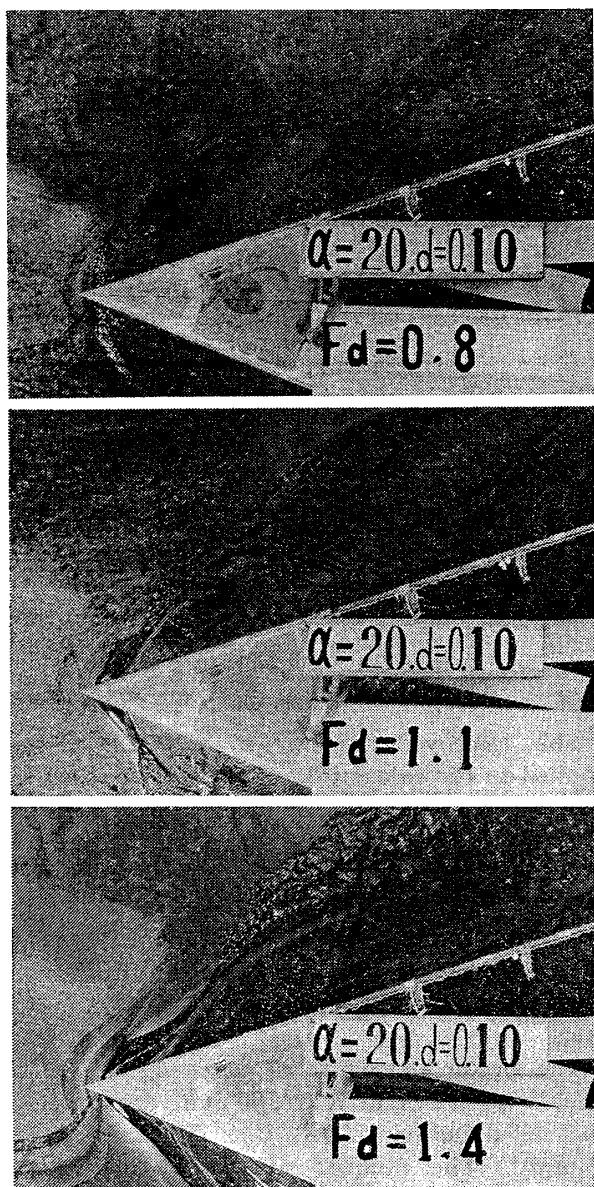


Fig. 3 Wave pattern pictures of a wedge model of $\alpha=20^\circ$

6.2 Wave formation

Wave pattern pictures around a wedge model of $\alpha=20^\circ$, whose length is about 1.0 m, photographed at the towing tank are present in Fig. 3. The foremost free surface shock wave (FSSW) is round-shaped and it is transformed into straight-lined at the Froude number (F_d) greater than 0.95. Then the angle of the foremost wave crest line to the centerline is decreased with the increase of F_d .

The computed wave height contours are shown in Fig. 4. The qualitative variation of wave formation above-described is present in this figure. Comparing these contours to the experimental ones in Ref. 3), it is noted that the computed wave height is about 70% of the measured and that the computed location of wave crest is shifted slightly backward. These are presumably due to truncation error, numerical dissipation and phase error caused by the numerical scheme. Perspective views of wave formation are present in Figs. 5 and 6, in which wave height is nondimensionalized by the reference length of $H(=U^2/2g)$ and somewhat exaggerated and

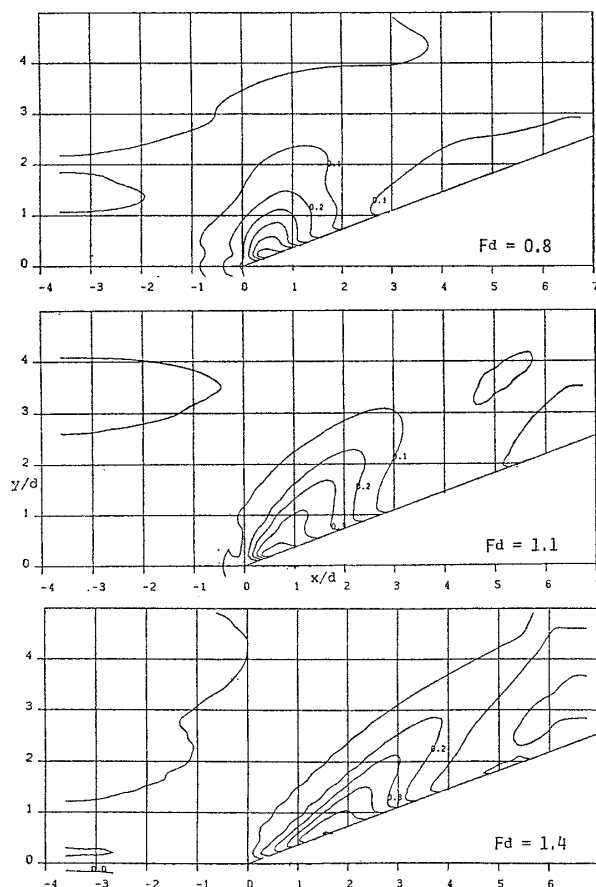


Fig. 4 Wave height contours around a wedge model of $\alpha=20^\circ$ calculated by the donor-cell-SOR method (at intervals of $0.1H$)

that of Fig. 6 is two-times magnified in comparison to Fig. 5. The formation of the foremost and partly the second waves are in good accordance

with the observed (Fig. 3).

Wave pattern pictures, computed wave height contours and perspective views for the case of $\alpha=45^\circ$ are present in Figs. 7 through 10. The foremost wave keeps to be round-shaped in the wide range of advance speed and is not transformed into straight-lined, i.e., the foremost wave is almost always normal FSSW, as seen in Fig. 7 and 8. With the increase of F_d the normal FSSW around the bow is enlarged and the wave slope on the forward face becomes steep, which will cause breaking of wave crest and unsteady

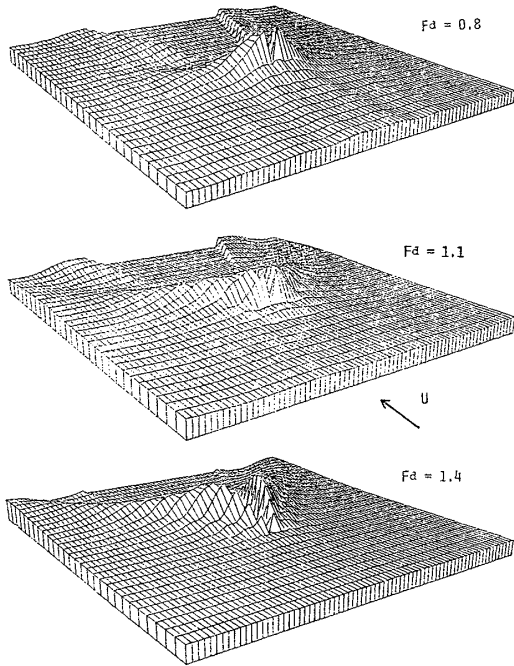


Fig. 5 Perspective views of wave configuration of a wedge model of $\alpha=20^\circ$ calculated by the donor-cell-SOR method (wave height is non-dimensionalized by H)

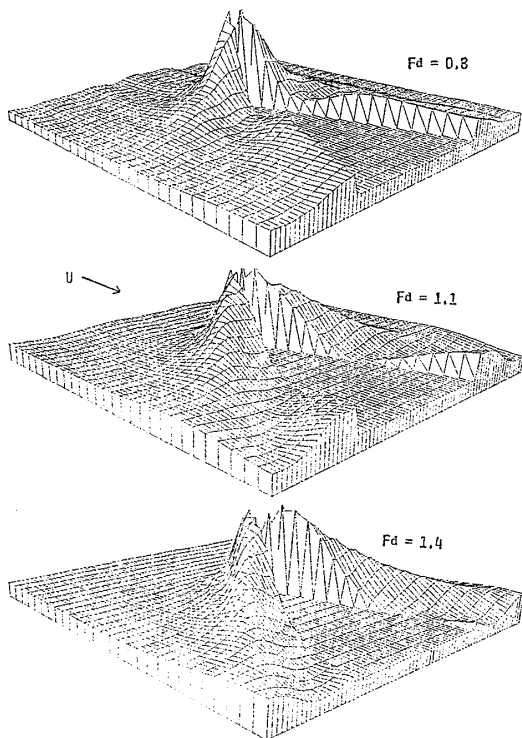


Fig. 6 Same as Fig. 5 (wave height is two-times magnified)

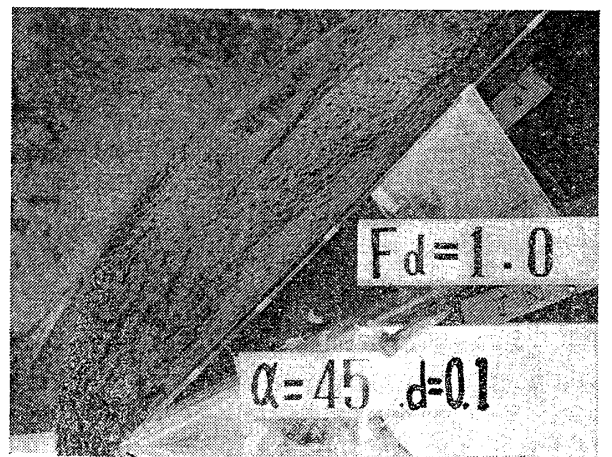
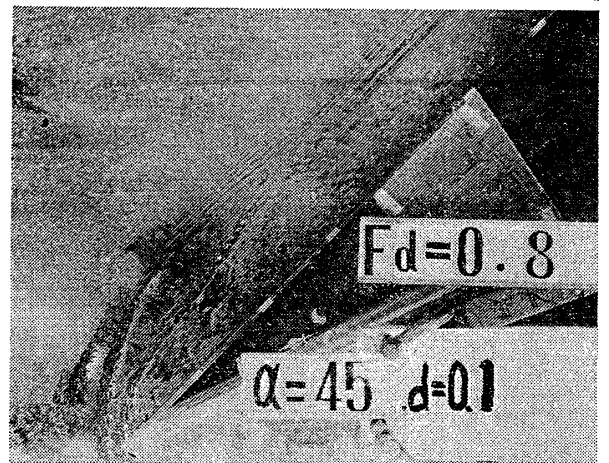
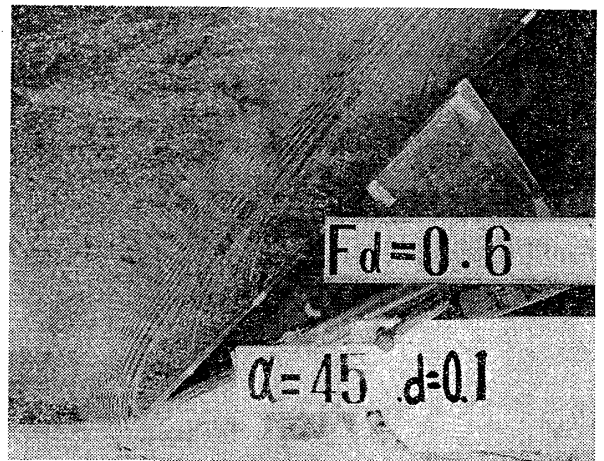


Fig. 7 Wave pattern pictures of a wedge model of $\alpha=45^\circ$

fluctuation of the free surface at high speed of advance. The wave height in the perspective views is nondimensionalized in the same way with the case of $\alpha=20^\circ$, and therefore, the wave height seen in Figs. 9 and 10 is nearly invariant, i.e., the maximum wave height is from 70% to 90% of H . This indicates that the wave height at the bow approaches very close to H and that in consequence the wave slope on the forward face is relatively very steep at high speed of advance.

FSSW is supposed to have four time-developing stages as described in Ref. 3), namely, 1) formation of very steep nonlinear waves, 2) breaking of wave crest and energy deficit, 3) diffusion of energy deficit with turbulence and sometimes air-entrainment on the free surface, and 4) formation of momentum-deficient wake far behind. The first stage is wave making ruled by Froude number and the followings are complicated and may suffer from the effect of viscosity. The present computation can explain the fluid mechanism of the first stage, which is

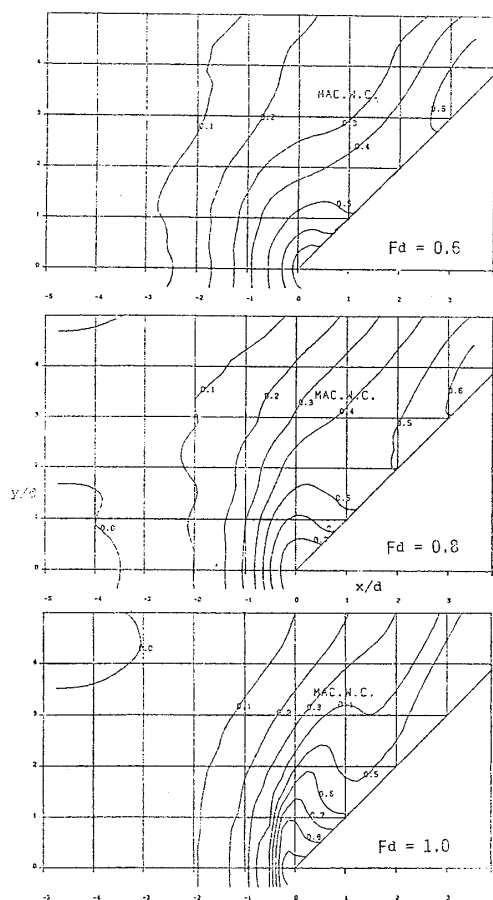


Fig. 8 Wave height contours around a wedge model of $\alpha=45^\circ$ calculated by the donor-cell-SOR method (wave height is nondimensionalized by H)

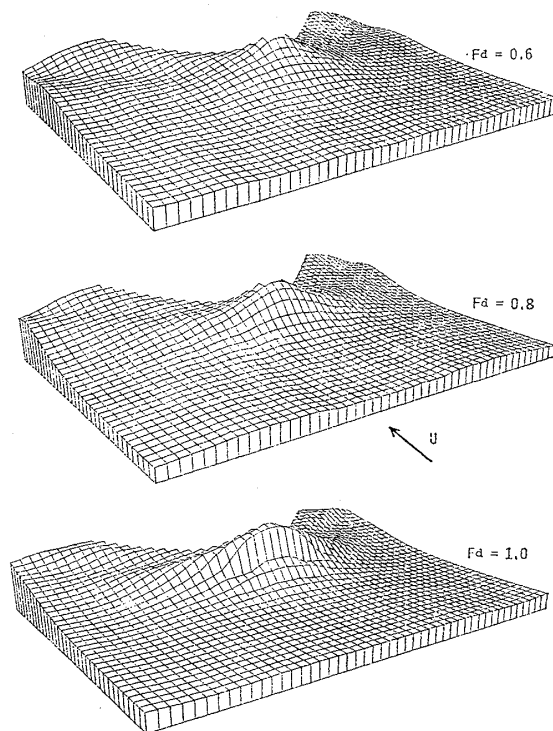


Fig. 9 Perspective views of wave configuration of a wedge model of $\alpha=45^\circ$ calculated by the donor-cell-SOR method (wave height is nondimensionalized by H)

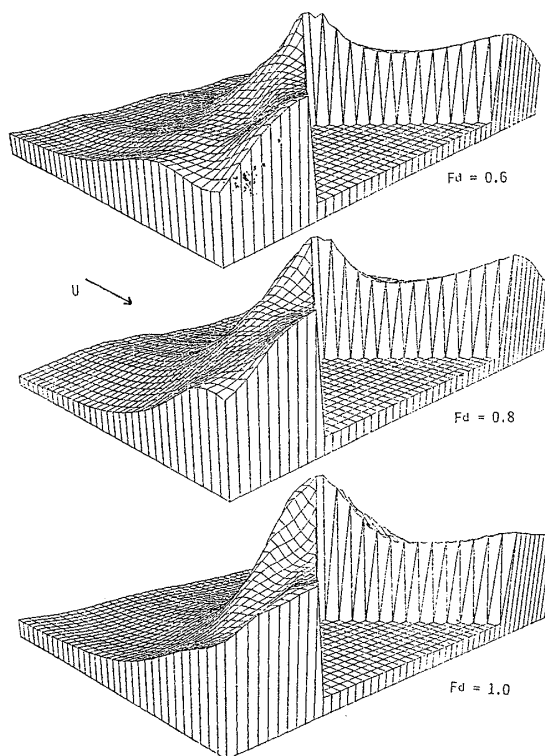


Fig. 10 Same as Fig. 9 (wave height is two-times magnified)

the most substantial for FSSW, and cannot demonstrate the subsequent stages, to which considerable efforts must be devoted.

6.3 Velocity and pressure distributions

Vertical fluid velocity distributions are present in Fig. 11 for the case of $\alpha=45^\circ$. The velocity component u reaches to more than 40% of the speed of uniform stream in the region where the wave is high. The extremely steep variation of vertical distribution of u near the free surface at the wave front seen in Fig. 24 of Ref. 3) is not realized in the computed result. This discord is attributed to the coarse cell dimension and the numerical dissipation as well as the complicated aspects of real phenomena (stages 2 to 3) that TUMMAC-I cannot take into consideration.

The calculated pressure distribution in the water is present in Fig. 12. The pressure must be in-between the two solid lines ④ and ③, which are the pressure distribution when waves do not exist and the hydrostatic distribution, respectively. When the waves have the same

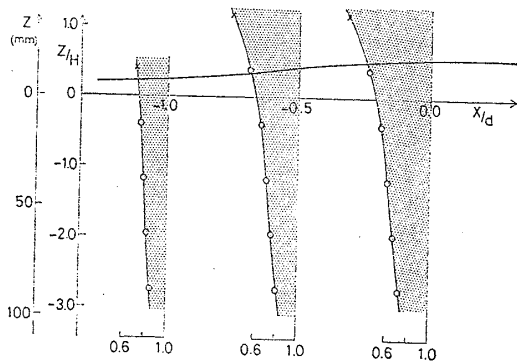


Fig. 11 Vertical distribution of calculated velocity component $1+u/U$ (wedge model of $\alpha=45^\circ$, $d=0.1$ m $F_a=0.8$, $y/d=1.0$)

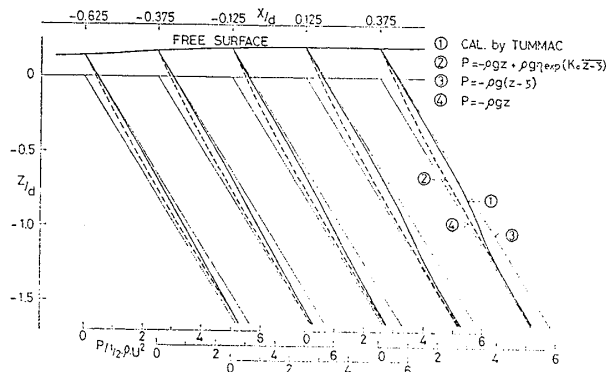


Fig. 12 Calculated pressure distribution on the vertical plane at $y/d=1.125$ (wedge model of $\alpha=45^\circ$, $F_a=0.8$)

property with nonlinear shallow water waves, the pressure distribution coincides with ③,

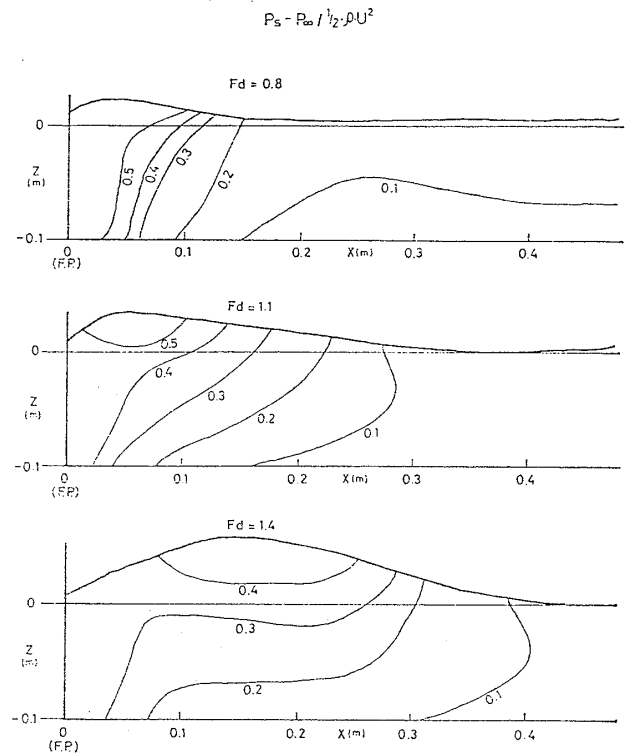


Fig. 13 Calculated pressure distribution on wedge surface (wedge model of $\alpha=20^\circ$, $d=0.1$ m)

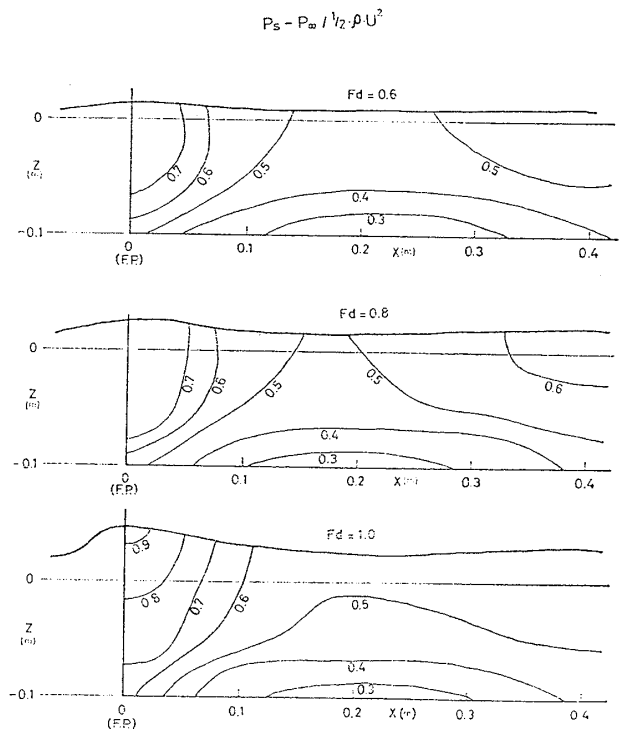


Fig. 14 Same as Fig. 13 (wedge model of $\alpha=45^\circ$, $d=0.1$ m)

and when they have the property of deep water waves, it coincides with the dotted curve ② which is drawn under the postulation that wave number K_0 is g/U^2 . The computed curve ① is in-between ② and ③, and it is very close to the hydrostatic distribution near the free surface. The presence of the hydrostatic pressure distribution revealed in the experimental results³⁾ is also demonstrated by the computation.

The computed pressure distributions on the surface of the wedge models are shown in Figs. 13 and 14. The variation of wave formation due to changes of advance speed and wedge angle is closely connected with the pressure distribution. Although the accuracy cannot be examined because of the lack of measured pressures, the resistance of the body can be estimated by integrating these distributions, which will be very useful for the design of the body configuration, i.e., hull form design, in future.

7. Conclusion

The numerical solution method TUMMAC-I for free surface motions around advancing wedge models in deep water is improved by employing the donor-cell differencing and the SOR method. The improved method gives stable solutions at various computational conditions more easily than the method in the previous paper, although the degree of accuracy is not very satisfactory.

The steep wave generation in the near-field of advancing floating bodies, which is the first and substantial stage of nonlinear wave making phenomenon called free surface shock wave, can be demonstrated by the TUMMAC-I. When this method is further developed into an advanced one which can be applied to ships of arbitrary

hull forms, the hull form design procedures will become more rigorous and economical.

Acknowledgement

The authors wish to express their thanks to Mr. K. Aoki and Mr. Y. Tsuchiya, graduate student and technical staff, respectively, of the University of Tokyo, for their supports in some computations and drawings. They are also indebted to Mr. A. Suzuki of IHI for his discussions in the course of this work. The computations were carried out by the computer system composed of several M200H of the Computer Center, the University of Tokyo. This research is partly supported by the Grant-in-Aid for Cooperative Research of the Ministry of Education, Science and Culture.

References

- 1) Suzuki, A. et al.: Numerical Analysis of Free Surface Shock Waves around Bow by Modified MAC-Method (First Report), J. Soc. Naval Arch. Japan, Vol. 150 (1981).
- 2) Miyata, H. et al.: Numerical Explanation of Nonlinear Nondispersive Waves around Bow, Proc. 3rd. Intern. Conf. Numerical Ship Hydrodynamics, (1981).
- 3) Miyata, H. et al.: Characteristics of Free Surface Shock Waves around Wedge Models (Second Report), J. Soc. Naval Arch. Japan, Vol. 151 (1982).
- 4) Roache, P. J.: Computational Fluid Dynamics, Hermosa Publishers, (1976).
- 5) Fromm, J. E.: Time Dependent Flow of an Incompressible Viscous Flow, Methods in Computational Physics, Vol. 3, Academic Press, (1964).